



Contents lists available at ScienceDirect

## Pattern Recognition

journal homepage: [www.elsevier.com/locate/pr](http://www.elsevier.com/locate/pr)

## Learning AAM fitting through simulation

Jason Saragih<sup>a,b,\*</sup>, Roland Göcke<sup>a,c</sup><sup>a</sup>Research School of Information Sciences and Engineering, College of Engineering and Computer Science, The Australian National University, Canberra, ACT 0200, Australia<sup>b</sup>Robotics Institute, Carnegie Mellon University, Pittsburgh, USA<sup>c</sup>Human-Computer Communication Laboratory, Faculty of Information Sciences and Engineering, University of Canberra, Canberra, ACT 2601, Australia

## ARTICLE INFO

## Article history:

Received 29 January 2009

Received in revised form 16 April 2009

Accepted 20 April 2009

## Keywords:

Active appearance model

Fitting

Discriminative

Linear model

## ABSTRACT

The active appearance model (AAM) is a powerful method for modeling and segmenting deformable visual objects. The utility of the AAM stems from two fronts: its compact representation as a linear object class and its rapid fitting procedure, which utilizes fixed linear updates. Although the original fitting procedure works well for objects with restricted variability when initialization is close to the optimum, its efficacy deteriorates in more general settings, with regards to both accuracy and capture range. In this paper, we propose a novel fitting procedure where training is coupled with, and directly addresses, AAM fitting in its deployment. This is achieved by simulating the conditions of real fitting problems and learning the best set of fixed linear mappings, such that performance over these simulations is optimized. The power of the approach does not stem from an update model with larger capacity, but from addressing the whole fitting procedure simultaneously. To motivate the approach, it is compared with a number of existing AAM fitting procedures on two publicly available face databases. It is shown that this method exhibits convergence rates, capture range and convergence accuracy that are significantly better than other linear methods and comparable to a nonlinear method, whilst affording superior computational efficiency.

© 2009 Elsevier Ltd. All rights reserved.

## 1. Introduction

First proposed by Edwards et al. [1], the active appearance model (AAM) has attracted much interest in the computer vision community for modeling and segmenting deformable visual objects. The method makes ingenious use of linear subspaces, allowing a compact representation of both shape and texture. Coupled with an efficient fitting procedure, the AAM has found utility in many computer vision problems, ranging from face animation [2] and medical image analysis [3], to industrial vision problems [4].

The AAM's rapid fitting stems from the utility of *fixed* linear update models. Despite its simplicity, the linear update model has been shown to approximately capture the relationship between the AAM's texture residual and the optimal parameter updates [1,5]. However, this relationship holds only loosely, as it depends on the current shape and texture parameters [6]. As such, extensions to AAM fitting have diverged into two camps. In the first, improved

fitting performance is attained by building feature vectors that better adhere to a linear relationship with the parameter updates [7,8]. Proponents of the second camp reformulate the analytic fitting problem such that the linear update model is better justified [6,9,10]. To reduce computational complexity, these methods usually make some assumptions about the forms of the analytic updates.

In this work, a new fitting procedure is proposed that couples training and testing through simulations of real fitting conditions. The method learns a set of *fixed* linear update models, each of which accounts for different distributions of the AAM parameters about their optimum, throughout the iterative fitting procedure. As these updates are fixed, and by virtue of their sequential application to the image, this approach affords an efficient evaluation.

The outline of this paper is as follows. In Section 2, a brief overview of related work is presented. Next, we present our approach for AAM fitting in Section 3, addressing implementation complexities in Sections 3.1 and 3.2. Empirical evaluations are presented in Section 4. We conclude in Section 5 with additional remarks and directions for future work.

## 2. Background

The AAM's intrinsic variations in shape and texture of deformable visual objects as a linear combination of basis modes of variation

\* Corresponding author at: Research School of Information Sciences and Engineering, College of Engineering and Computer Science, The Australian National University, Canberra, ACT 0200, Australia.

E-mail addresses: [jsaragih@cs.cmu.edu](mailto:jsaragih@cs.cmu.edu) (J. Saragih), [roland.goecke@ieee.org](mailto:roland.goecke@ieee.org) (R. Göcke).

that are composed with a global transformation<sup>1</sup> :

$$S(\mathbf{q}_s): \mathfrak{R}^{n_s} \mapsto \mathfrak{R}^{2n} = s(\mathbf{I} \otimes \mathbf{R})(\boldsymbol{\mu}_s + \Phi_s \mathbf{p}_s) + \mathbf{1} \otimes \mathbf{t}, \quad (1)$$

$$T(\mathbf{q}_t): \mathfrak{R}^{n_t} \mapsto \mathfrak{R}^m = \alpha(\boldsymbol{\mu}_t + \Phi_t \mathbf{p}_t) + \beta \mathbf{1}, \quad (2)$$

where  $S$  and  $T$  denote the generative models for shape and texture, parameterized by  $\mathbf{q}_s = \{s, \mathbf{R}, \mathbf{t}, \mathbf{p}_s\}$  and  $\mathbf{q}_t = \{\alpha, \beta, \mathbf{p}_t\}$ , respectively. Here,  $\{\boldsymbol{\mu}_s, \Phi_s\}$  and  $\{\boldsymbol{\mu}_t, \Phi_t\}$  denote the mean and basis of variations of the shape and texture, which are typically obtained by applying PCA on the training data. The intrinsic shape is composed with a similarity transform, parameterized by a global scaling  $s$ , a rotation  $\mathbf{R}$  and a translation  $\mathbf{t}$ . The intrinsic texture is scaled by a global gain  $\alpha$  and biased by  $\beta$ . Finally,  $n$  denotes the number of points in the model's shape and  $m$  denotes the number of pixels in the model's texture.

AAM fitting is the process of finding the model parameters  $\mathbf{p} = \{\mathbf{q}_s, \mathbf{q}_t\}$  which best fit an AAM to an image  $I$ . This is usually an iterative procedure that sequentially updates the model parameters  $\mathbf{p}$  through an update function:

$$\Delta \mathbf{p} = U(\diamond; \mathbf{p}) \circ F(I; \mathbf{p}). \quad (3)$$

Here,  $F$  is a feature extraction function that represents the image  $I$  from the perspective of the AAM at its current parameter settings and  $\Delta \mathbf{p}$  are the updates to be applied to the current parameters.  $U$  is typically chosen to be the linear update model:

$$U(\mathbf{f}; \mathbf{p}): \mathfrak{R}^m \mapsto \mathfrak{R}^{n_s+n_t} = \mathbf{G}\mathbf{f} + \mathbf{b} \quad \text{where } \mathbf{f} = F(I; \mathbf{p}), \quad (4)$$

although nonlinear mappings have also been used [11,12]. In any case, a good coupling between  $U$  and  $F$  is required to ensure good predictions of the updates. There are two general approaches to AAM fitting: *generative* and *discriminative*. In the following, we will briefly discuss each in turn.

### 2.1. Generative fitting

Generative methods pose fitting as the minimization of some measure of error between the AAM's synthesized texture and the warped image. The most common measure of fit is the least squares error [5,6,10]:

$$Q(\mathbf{p}) = \|T(\mathbf{q}_t) - I \circ W \circ S(\mathbf{q}_s)\|^2, \quad (5)$$

where  $W$  is a function that warps pixel locations in the reference frame onto the image. Robust variants of this objective have been used also, in which case the problem takes the form of a continually reweighted least squares problem [13]. In general, the Gauss–Newton method has become the optimizer of choice, where at each iteration the parameters are updated using the linear form in Eq. (4). However, a naive implementation is computationally expensive as  $(\mathbf{G}, \mathbf{b})$  depends on  $\mathbf{p}$ . As such, most generative approaches to AAM fitting either assume some parts of the update computation are fixed or reformulate the problem such that they are.

The original generative approach in [5] assumes that the Jacobian of Eq. (5) is fixed, allowing  $(\mathbf{G}, \mathbf{b})$  to be precomputed. More recently, in a method coined adaptive AAM [10], the fixed Jacobian (FJ)

assumption is relaxed by decomposing it and assuming only the component pertaining to the derivative of the warping function is fixed. The resulting method exhibits improved accuracy; however, as the linear update model depends on the current texture parameters, the fitting procedure is computationally expensive.

Adaptations of the inverse-compositional image alignment [14] to AAM fitting has also attracted some interest. By reversing the roles of the image and the model in the fitting objective, the derivative of the warping function is fixed, resulting in significant computational savings. The project-out method [6], for example, minimizes the cost in a subspace orthogonal to the modes of texture variation, resulting in an analytically fixed linear update model. Despite being the fastest method to date, it works well only for objects exhibiting small amounts of variation, such as, for example, in person-specific face tracking [15]. This problem is partially addressed by the simultaneous method [9], which solves for the shape and texture parameters simultaneously. However, similar to the method in [10], its update model depends on the current texture parameters, again resulting in a computationally expensive fitting procedure.

### 2.2. Discriminative fitting

Although generative approaches have an intuitive appeal, they are optimally constructed for synthesis, rather than fitting. To address this drawback, a number of authors propose learning a fitting strategy discriminatively, where both aligned and misaligned examples are considered during training [1,7,12,16,17]. There are two general strategies in discriminative fitting. The first is to learn an objective function with desirable properties that promote convergence of a gradient descent type search to the desired optimum [16,17]. The second is to learn a fixed mapping between the features  $F(I; \mathbf{p})$  and the parameter updates  $\Delta \mathbf{p}$  [1,7,12], given a training set of perturbed model parameters:

$$\{F(I_i; \mathbf{p}_i^* - \Delta \mathbf{p}_i), \Delta \mathbf{p}_i\}_{i=1}^d, \quad (6)$$

where  $\mathbf{p}_i^*$  is the optimal parameter setting for the  $i$ th sample and  $d$  is the total number of perturbations in the training set. The advantage of the second approach is that no nonlinear optimization is required during fitting, potentially leading to an efficient fitting procedure.

In the original AAM formulation [1], the linear update model was shown to approximately explain the relationship between the AAM's texture residual:

$$F(I; \mathbf{p}) = T(\mathbf{q}_t) - I \circ W \circ S(\mathbf{q}_s) \quad (7)$$

and the parameter updates  $\Delta \mathbf{p}$ , around the optimal parameter settings  $\mathbf{p}^*$  for a given image. The update  $U$  is easily found through linear regression on the data set in Eq. (6). The direct appearance model method [8] affords better memory efficiency during training as well as improves fitting performance by using the PCA reduced texture residuals and predicts the shape directly from the texture. In [7], a linear relationship is learnt between the canonical projections of the texture residuals and parameter updates. The method utilizes canonical correlation analysis to find the subspaces which best adheres to a linear relationship. In [12], the mapping capacity is increased by using a boosted mapping function of weak learners.

Finally, it should be noted that a number of discriminative approaches to template tracking have been proposed recently with similar forms to the deformable model fitting methods described above. Examples of this include [18–20]. However, the application of such approaches to deformable model fitting requires a specialized treatment due to the higher dimensionality of the motion model and the typically larger variability of intrinsic appearance.

<sup>1</sup> Notation: Vectors are written in lowercase bold and matrices in uppercase bold, where  $\mathbf{1}$  denotes the all one vector and  $\mathbf{I}$  the identity matrix. Greek letters denote either vectors or matrices depending on context. The Kronecker (tiling) product is written using  $\otimes$ . The  $\text{vec}\{\cdot\}$  operator vectorizes a matrix by stacking its columns. Functions are written in upper case with  $\circ$  denoting their composition. When composing functions with multiple parameters,  $\diamond$  denotes a place-holder, i.e.:  $A(B(\mathbf{x}); \mathbf{y}) = A(\diamond; \mathbf{y}) \circ B(\mathbf{x})$ .

### 3. Learning the mappings through simulation

The major drawbacks of current AAM fitting methods are

- A fixed linear update model cannot accurately account for the various error terrains about the optimum in different images.
- Adapting the update model to the image at hand requires a costly process of re-calculating it for every iteration.
- Increasing the complexity of the mapping function in a discriminative setting may lead to issues with generalizability as well as computational complexity.

In this work, the drawbacks of a fixed linear model are addressed whilst maintaining efficiency. To this end, we propose learning the entire fitting procedure in a discriminative framework rather than extracting the update model, or an approximation thereof, from a generative stand point. Learning is performed on examples of real fitting scenarios, simulated on the training data.

Consider the class of linear update models that utilize the additive parameter update:  $\mathbf{p} \leftarrow \mathbf{p} + \Delta\mathbf{p}$ . If no adjustments to the parameters are performed between iterations, such as projections onto the three standard deviations ellipsoid, then the effective parameter adaptation after  $k$  iterations is given by

$$\mathbf{p} \leftarrow \mathbf{p} + \sum_{i=1}^k \Delta\mathbf{p}_i. \quad (8)$$

Utilizing a different update model in each iteration, the parameter updates can be written as

$$\Delta\mathbf{p}_i = \mathbf{G}_i F \left( I; \mathbf{p} + \sum_{j=1}^{i-1} \Delta\mathbf{p}_j \right) + \mathbf{b}_i, \quad (9)$$

where  $\{\mathbf{G}_i, \mathbf{b}_i\}$  is the *fixed* update model for the  $i$ th iteration. Given the training set in Eq. (6), the optimal update models for all  $k$  iterations can be found by minimizing a cost function of the form

$$Q(\mathbf{m}) = \frac{1}{d} \sum_{j=1}^d C_D(I_j, \mathbf{p}_j, \mathbf{s}_j^*; \mathbf{m}), \quad (10)$$

where  $\mathbf{s}_j^*$  are the hand-labeled annotations for the  $j$ th training sample:  $\mathbf{p}^* = \min_{\mathbf{q}} \|\mathbf{s}^* - S(\mathbf{q}_s)\|^2$ . The parameters of this cost function are the update models themselves:

$$\mathbf{m} = [\text{vec}(\mathbf{G}_1); \dots; \text{vec}(\mathbf{G}_k); \mathbf{b}_1; \dots; \mathbf{b}_k]. \quad (11)$$

The distance function  $C_D$  in Eq. (10) penalizes the difference between the manually annotated shapes and the predicted model's shape after  $N_i$  iterations<sup>2</sup> :

$$C_D(I, \mathbf{p}, \mathbf{s}^*; \mathbf{m}) = \frac{1}{2} \left\| S \left( \mathbf{p} + \sum_{i=1}^k \Delta\mathbf{p}_i \right) - \mathbf{s}^* \right\|^2. \quad (12)$$

Compared to texture based error measures, commonly used in generative AAM fitting, this distance function better encompasses all available knowledge about the optimal parameter setting, i.e. the hand-labeled annotations. With this formulation, the training

procedure essentially simulates real fitting problems on the set of training images and perturbations. If at deployment, the unseen images and their perturbations resemble those in the training set, then the fitting performance of the minimizer of Eq. (10) can be expected to approach that at training.

Having trained the update models that minimize Eq. (10), AAM fitting then proceeds as outlined in Algorithm 1. Notice that no checks need to be made regarding the reduction of texture error or the magnitude of the parameter updates. Fitting is simply performed for all trained iterations with no early termination.

**Algorithm 1.** Discriminative iterative AAM fitting.

**Require**  $I, \{U_1, \dots, U_k\}$  and  $\mathbf{p}$

- 1: **for**  $i = 1$  to  $k$  **do**
- 2:      $\mathbf{f} = F(I; \mathbf{p})$  {Get feature vector}
- 3:      $\Delta\mathbf{p} = \mathbf{G}_i \mathbf{f} + \mathbf{b}_i$  {Calculate updates}
- 4:      $\mathbf{p} \leftarrow \mathbf{p} + \Delta\mathbf{p}$  {Update current parameters}
- 5: **end for**
- 6: **return**  $\mathbf{p}$

Compared to the training procedure of generative methods, finding the optimal update models by minimizing Eq. (10) presents a number of difficulties. Firstly, the cost function is inherently nonlinear with many local minima, due to the composition of the updates with the feature vectors and the nonlinear relationship between the pixel intensities and the warping parameters. Secondly, standard numerical optimization techniques are not computationally practical for this problem. Since the parameter updates at each iteration depend on the update models for all previous iterations, the analytic gradient of Eq. (12) is in general extremely complex, resulting in an impractical computational burden. This matter is made worse by the potentially large number of training samples required to ensure good generalizability of the update models. In the following sections, we discuss methods to make the optimization computationally tangible as well as allowing a good *local* solution to the nonlinear problem in Eq. (10) to be obtained.

#### 3.1. Stochastic gradient descent

The training set in Eq. (6) is generally obtained by sampling from a distribution that approximates the true distribution of perturbation errors encountered in deployment [12,17]. Since the training set consists of an unbounded number of samples for each training image, we recast the problem as one of online estimation, where each sample, or a small set of them, is treated as it arrives. Online estimation is essentially a stochastic optimization problem, since only noisy objective function evaluations are available due to restrictions on the sample set size at each instance. There are a number of advantages of online/stochastic learning over batch learning.<sup>3</sup> For example, it has been widely reported that it can reduce training time [21], has the ability to escape from *shallow* local minima [22], minimizes the true risk rather than the empirical risk [23], requires far less memory, and it does not require the number of samples to be chosen a priori.

Given the instantaneous cost function at time  $t$ :

$$C_t(\mathbf{m}) = \frac{1}{n_b} \sum_{j=1}^{n_b} C_D(I_j, \mathbf{p}_j, \mathbf{s}_j^*; \mathbf{m}), \quad (13)$$

<sup>2</sup> Note that, here, we consider mappings only over the shape parameters such that  $\mathbf{p} = \mathbf{q}_s$ .

<sup>3</sup> Batch learning minimizes the empirical risk over the whole training set simultaneously.

where  $n_b$  is the *mini-batch* size, stochastic optimization then proceeds by first calculating the gradient:

$$\mathbf{d}_t = \frac{1}{n_b} \sum_{j=1}^{n_b} \frac{\partial C_{D_j}}{\partial \mathbf{m}} \quad (14)$$

then updating the model parameters in a steepest descent fashion:

$$\mathbf{m}_{t+1} = \mathbf{m}_t - \eta_t \mathbf{d}_t, \quad (15)$$

where the step size  $\eta$  is scheduled such that

$$\eta_t > 0; \quad \eta_t \rightarrow 0 \text{ as } t \rightarrow \infty; \quad \sum_{t=0}^{\infty} \eta_t = \infty \text{ and } \sum_{t=0}^{\infty} \eta_t^2 < \infty \quad (16)$$

to guarantee convergence to a local minimum. However, the deterministic gradient of Eq. (13) cannot be trivially evaluated due to the dependence of the updates on those of previous iterations. To see this, note that the deterministic gradient of  $C_D$  is given by

$$\frac{\partial C_D}{\partial \mathbf{m}} = \frac{\partial C_D}{\partial \mathbf{z}} \frac{\partial \mathbf{z}}{\partial \mathbf{m}}, \quad (17)$$

where  $\mathbf{z} = [\Delta \mathbf{p}_1; \dots; \Delta \mathbf{p}_{N_i}]$  is the concatenation of the parameter updates of all iterations. The derivative  $\partial C_D / \partial \mathbf{z}$  can be easily computed from Eqs. (12) and (1). Now, consider the simplest case, where

$$F(I; \mathbf{p}) = I \circ W \circ S(\mathbf{p}). \quad (18)$$

With this feature vector, the derivative of the  $j$  th parameter update with respect to the bias vector of the  $k$  th iteration is given by the following recursive form:

$$\frac{\partial \Delta \mathbf{p}_j}{\partial \mathbf{b}_k} = \begin{cases} \mathbf{0} & \text{if } j < k, \\ \mathbf{I} & \text{if } j = k, \\ \mathbf{G}_j \frac{\partial F}{\partial \mathbf{p}} \left( \sum_{i=1}^{j-1} \frac{\partial \Delta \mathbf{p}_i}{\partial \mathbf{b}_k} \right) & \text{if } j > k, \end{cases} \quad (19)$$

where the derivative of the warped image  $\partial F / \partial \mathbf{p}$  is evaluated at  $\mathbf{p} + \sum_{i=1}^{j-1} \Delta \mathbf{p}_i$ . The derivative with respect to the  $k$  th gain matrix is given by

$$\frac{\partial \Delta \mathbf{p}_j}{\partial \mathbf{G}_k} = \frac{\partial \Delta \mathbf{p}_j}{\partial \mathbf{b}_k} \otimes F \left( \mathbf{p} + \sum_{i=1}^{k-1} \Delta \mathbf{p}_i \right). \quad (20)$$

The evaluation of these partial derivatives is computationally intensive and memory demanding. Furthermore, the complexity of evaluating these partials grows exponentially with the number of iterations  $k$ . In fact, we found that for  $k > 3$ , the optimization becomes impractical on typical hardware. This problem is amplified with the use of more sophisticated feature vectors, especially those that involve an adaptive normalization component.

To avoid the costly computation of deterministic gradients, we utilize simultaneous perturbation stochastic approximation (SPSA) [24]. This method computes stochastic gradients of a function with as little as two function evaluations, allowing an efficient optimization procedure to be constructed. Specifically, the stochastic gradient of Eq. (13) is computed as follows:

$$\hat{\mathbf{d}}_t = \frac{1}{2\gamma_t} [C_t(\mathbf{q} + \gamma_t \Delta_t) - C_t(\mathbf{q} - \gamma_t \Delta_t)] \Delta_t, \quad (21)$$

where  $\Delta_t$  is a vector of random perturbations for each model parameter, independently generated from a zero-mean probability distribution satisfying the conditions in [25], for example the

Bernoulli  $\pm 1$  distribution with probability of 0.5 for each outcome. The perturbation magnitude  $\gamma_t$  requires similar conditions to  $\eta$  in Eq. (16) to guarantee convergence. Common choices for  $\eta_t$  and  $\gamma_t$ , which satisfy these conditions, are

$$\eta_t = \frac{\eta}{(a+t)^\alpha} \quad \text{and} \quad \gamma_t = \frac{\gamma}{t^\beta}, \quad (22)$$

where  $(\eta, \gamma)$  are the initial values and  $(\alpha, \beta)$  are the decay rates for the step size and perturbation magnitudes, respectively. Here,  $a$  is a stabilizing constant that allows a larger initial step size  $\eta$ , whilst avoiding instabilities in early iterations. We should note here that since the elements of  $\mathbf{m}$  have very different magnitudes, depending on which element of  $\mathbf{p}$  they map onto, they are first scaled according to the maximum expected perturbation of their respective AAM parameter  $\mathbf{p}$  before applying the update in Eq. (15). Finally, the performance of SPSA depends on the choices made for the free variables  $(\eta, \gamma, a, \alpha, \beta)$ . A practical guide for choosing these variables is given in [26].

By performing online estimation using SPSA, the noise in our system is amplified: the noisy gradient approximation is made on noisy cost evaluations  $C_t$ . As such, it is important to choose the SPSA parameters such that the fluctuations due to noise do not overwhelm the optimization process and cause instability. Estimation noise can be further reduced by taking an average of a number of stochastic gradient approximations [24]. In practice, optimization is run for a number of iterations on different parameter settings, choosing the one which induces the best efficiency per update, without making the optimization unstable.

### 3.2. Spread minimized initialization

Although noise in the stochastic estimation helps the optimization escape from local minima with shallow terrain, it may still terminate in a poor local minimum. A good initialization for the update models is, therefore, required to encourage good solutions to be obtained by the optimization process. For this, consider first that we utilize only linear models at every iteration. Therefore, the performance of this method is limited by the estimation capacity of the linear model in the final iteration. However, as all update models are learnt simultaneously, all update models except the last one act as *sample redistributors* such that the distribution of the samples around their optimum in the last iteration can be well accounted for by the final linear update model.

With this in mind, we cite the results by Cootes et al. [5], that the relationship between the texture residuals and the parameter updates is close to linear only within a small region around the optimum of each AAM parameter. In fact, this relationship has been shown to persist, though to a lesser extent, even for the simple warped texture feature [27]. As such, we argue that a reasonable initialization for the optimization in Section 3.1 is one that reduces the spread of the samples about their optimum.

To this end, we propose performing a greedy learning process for each iteration, in a sequential manner, each of which aims to minimize the spread of samples about their respective optimum, given the samples that have been updated by previous iterations. We achieve this by learning a linear regressor for every parameter independently, by minimizing the following cost function for each:

$$C_{\text{greedy}}(\mathbf{g}, b) = \frac{1}{d} \sum_{j=1}^d C_{\text{asy}}(I_j, \mathbf{p}_j, \Delta p_j; \mathbf{g}, b) + \frac{\lambda}{2} \|\mathbf{g}\|^2, \quad (23)$$

where  $\lambda$  is a regularization constant and

$$C_{\text{asy}}(I, \mathbf{p}, \Delta p; \mathbf{g}, b) = \frac{1}{\varepsilon - (\mathbf{g}^T \mathbf{f} + b - \Delta p)^2}. \quad (24)$$



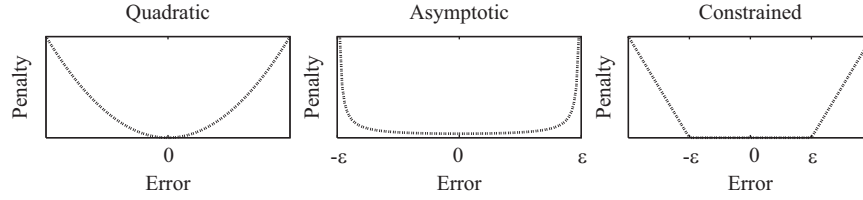


**Fig. 1.** Quadratic, asymptotic and constrained penalizers. The asymptotic penalizer places more weight on samples far from the optimum compared to a quadratic penalizer. Compared to the constrained penalizer, the asymptotic penalizer minimizes the spread of samples rather than their error margin only.

Here,  $\mathbf{f}$  is as in Eq. (4) and

$$\varepsilon = \max(\Delta p_j^2) + \delta, \quad j \in \{1, \dots, k\}, \quad \delta \in \mathfrak{R}^+. \quad (25)$$

Note that the full update model is composed of the regressor for each parameter:

$$\mathbf{G} = [\mathbf{g}_1^T; \dots; \mathbf{g}_{n_s}^T] \quad \text{and} \quad \mathbf{b} = [b_1; \dots; b_{n_s}], \quad (26)$$

where  $n_s$  is the total number of parameters.

Previously, we used a similar cost function as in Eq. (23) to train nonlinear parameter update mappings in [11]. It asymptotically penalizes the distance of each sample from its optimum, placing more emphasis on samples with large perturbations compared to, for example, the quadratic loss (see Fig. 1). Furthermore, this asymptotic penalizer is convex within the convex set:

$$|(\mathbf{g}, b) - \sqrt{\varepsilon} < \mathbf{g}^T \mathbf{f}_j + b - \Delta p_j < \sqrt{\varepsilon}; j = 1, \dots, d, \quad (27)$$

i.e. the intersection of  $d$  convex sets, each composed of the region between two parallel hyperplanes. Due to the choice of  $\varepsilon$  in Eq. (25), the null model  $((\mathbf{g}, b) \leftarrow \mathbf{0})$  lies within this convex region. As such, starting with the null model and performing steepest descent with a line search allows the globally optimum update model to be found. Unlike the optimization problem discussed in Section 3.1, the gradient of this cost function is easily computed:  $\partial C_{\text{asy}} / \partial b = \theta$  and  $\partial C_{\text{asy}} / \partial \mathbf{g} = \theta \mathbf{f}$ , where

$$\theta = 2r(\varepsilon - r^2)^{-2}, \quad r = \mathbf{g}^T \mathbf{f} + b - \Delta p. \quad (28)$$

We previously proposed a similar greedy learning objective in [28] using a constrained objective (see Fig. 1). However, that objective does not penalize samples within the margin, which may lead to the clustering of samples around the margin.

For optimization, we use the limited memory BFGS algorithm (L-BFGS) [29], a variant of the quasi-Newton optimizer BFGS, which avoids the cost of storing and updating the estimate of the cost function's Hessian inverse. Given the L-BFGS step direction  $\mathbf{d}$ , the line search is performed by solving

$$\alpha^* = \min_{\alpha} \frac{1}{d} \sum_{j=1}^d \frac{1}{\varepsilon - (\alpha[\mathbf{f}_j \ 1] \mathbf{d} + \mathbf{g}^T \mathbf{f}_j + b - \Delta p_j)^2} + \lambda \|\mathbf{d}\|^2 \alpha$$

$$\text{s.t. } 0 \leq \alpha \leq \min \left( \frac{\pm \sqrt{\varepsilon} - \mathbf{g}^T \mathbf{f}_j - b + \Delta p_j}{[\mathbf{f}_j \ 1] \mathbf{d}} \right), \quad j \in \{1, \dots, d\}, \quad (29)$$

where the sign of  $\sqrt{\varepsilon}$  is chosen to represent the asymptote in the direction of the update. The training procedure is summarized in Algorithm 2.

**Algorithm 2.** Greedy spread minimization.

**Require:**  $k$  and  $d$

- 1: **for**  $i = 1$  to  $k$  **do**
- 2:    $\{I_j, \mathbf{s}_j^*, \mathbf{p}_j\}_{j=1}^d$  {Sample training data}
- 3:   **for**  $j = 1$  to  $d$  **do**
- 4:      $\mathbf{f}_j = F(I_j, \mathbf{p}_j)$  {Get feature vector}
- 5:     **for**  $l = 1$  to  $i - 1$  **do**
- 6:        $\mathbf{p}_j \leftarrow \mathbf{p}_j + \mathbf{G}_l \mathbf{f}_j + \mathbf{b}_l$  {Update parameters}
- 7:     **end for**
- 8:      $\mathbf{f}_j = F(I_j, \mathbf{p}_j)$  {Get feature vector}
- 9:   **end for**
- 10: Calculate  $\{\varepsilon_1, \dots, \varepsilon_{N_p}\}$  {Eq. (25)}
- 11:  $(\mathbf{g}, b)_l \leftarrow \mathbf{0}$  for  $l \in \{1, \dots, n_s\}$  {Initialize}
- 12: **while** !converged( $\mathbf{G}_i, \mathbf{b}_i$ ) **do**
- 13:   **for**  $l = 1$  to  $n_s$  **do**
- 14:     Compute L-BFGS step  $\mathbf{d}_l$  {See [29]}
- 15:     Perform line search to get  $\alpha_l^*$  {Eq. (29)}
- 16:      $(\mathbf{g}, b)_l \leftarrow [\mathbf{g}; b]_l + \alpha_l^* \mathbf{d}_l$  {Update model}
- 17:   **end for**
- 18: **end while**
- 19: Assign update of  $i$  th iteration {Eq. (26)}
- 20: **end for**
- 21: **return**  $\mathbf{G}_1, \dots, \mathbf{G}_k$  and  $\mathbf{b}_1, \dots, \mathbf{b}_k$

## 4. Experiments

We conducted experiments on two publicly available face databases: the IMM face database [30] and the XM2VTS database [31]. The simulation learnt (SL) approach was compared against the fixed Jacobian method [5], project-out inverse-compositional method (POIC) [6], the efficient estimate of the simultaneous inverse-compositional method (SIC) [9] and the nonlinear discriminative (ND) method [11]. The performance of all methods was compared on these two databases, evaluated using 4-fold cross-validation, where each database was partitioned into four parts, in such a way, that test images contain unseen subjects only.

### 4.1. Databases

The IMM face database consists of 240 images of 40 subjects, exhibiting variations in pose, expression and lighting. Manual annotations of 58-landmarks are supplied with the database. The XM2VTS database consists of 2360 frontal images of 295 subjects with large inter-subject variability, including glasses, facial hair and race. A 68-landmark annotation of this database is publicly available from [32]. In both databases, we retained 95% of the intrinsic shape and texture variation. This gave an average of 19 modes of shape variation and 99 texture modes for the IMM database. The models built for the XM2VTS database exhibited on average 47 shape modes and 352 texture modes.

## 4.2. Simulation training

To generate the training set in Eq. (6), the AAM was randomly perturbed from its optimal parameter setting in each training image within  $\pm 10^\circ$  of rotation,  $\pm 0.1$  global scaling,  $\pm 20$  pixels translation and  $\pm 1.5$  standard deviations for the non-rigid shape parameters.

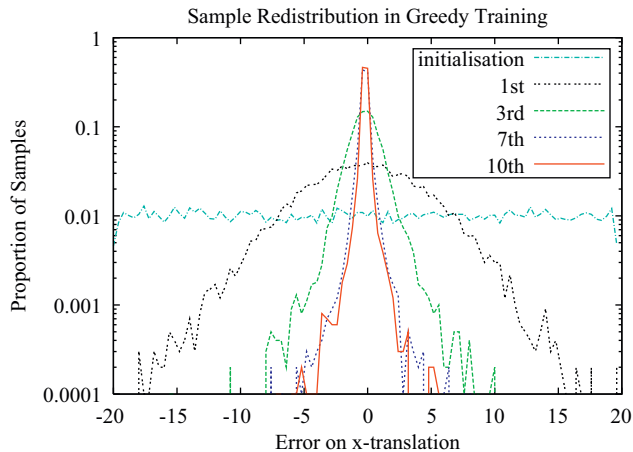


Fig. 2. Redistribution of samples about the  $x$ -translation optimum in the greedy training procedure on the IMM database. Legend denotes iteration.

This distribution of samples was chosen to mimic the initialization capacity of a generic detector. SL was trained for  $k = 10$  iterations using the normalized warped texture feature:

$$F(I; \mathbf{p}) = N \circ I \circ W \circ S(\mathbf{p}), \quad (30)$$

where  $N$  normalizes the warped texture to a mean of zero and a variance of one. The trained AAM drives only the shape parameters during fitting.

### 4.2.1. Greedy training

For model initialization, we used  $d = 2000$  samples in the procedure outlined in Algorithm 2. Fig. 2 illustrates the redistribution of samples throughout the greedy training process for the  $x$ -translation. A similar trend can be observed for the other parameters. As described in Section 3.2, the form of Eq. (23) places more emphasis on samples exhibiting large error. This is reflected in the figure where the spread of the samples about their optimum is reduced at each iteration. Notice that the reduction of sample spread between the 7th and 10th iteration is marginal, suggesting that the capacity of linear models has been exhausted, justifying the choice of  $k = 10$ .

### 4.2.2. Stochastic optimization

The stochastic optimization of all linear update models requires an appropriate choice of mini-batch size and gradient estimates such that the noise in the stochastic approximation does not make the optimization unstable. Empirically, we found that a mini-batch size of  $n_b = 50$  and  $n_g = 2$  gradient estimates gave a good balance between

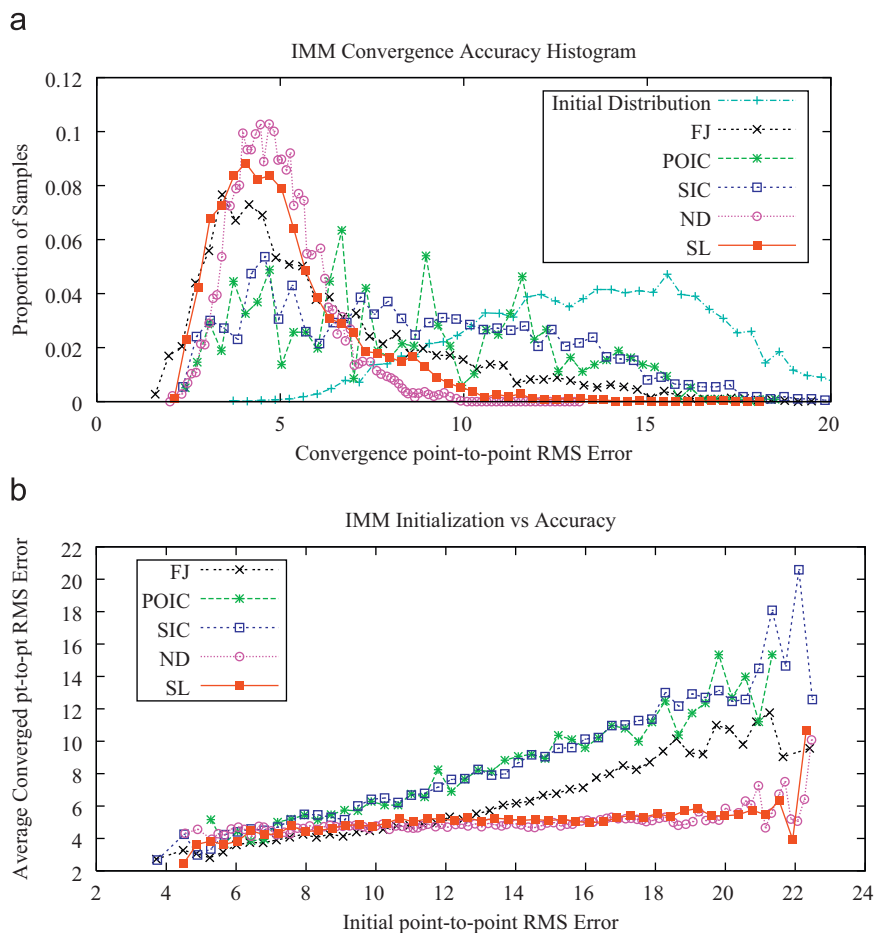
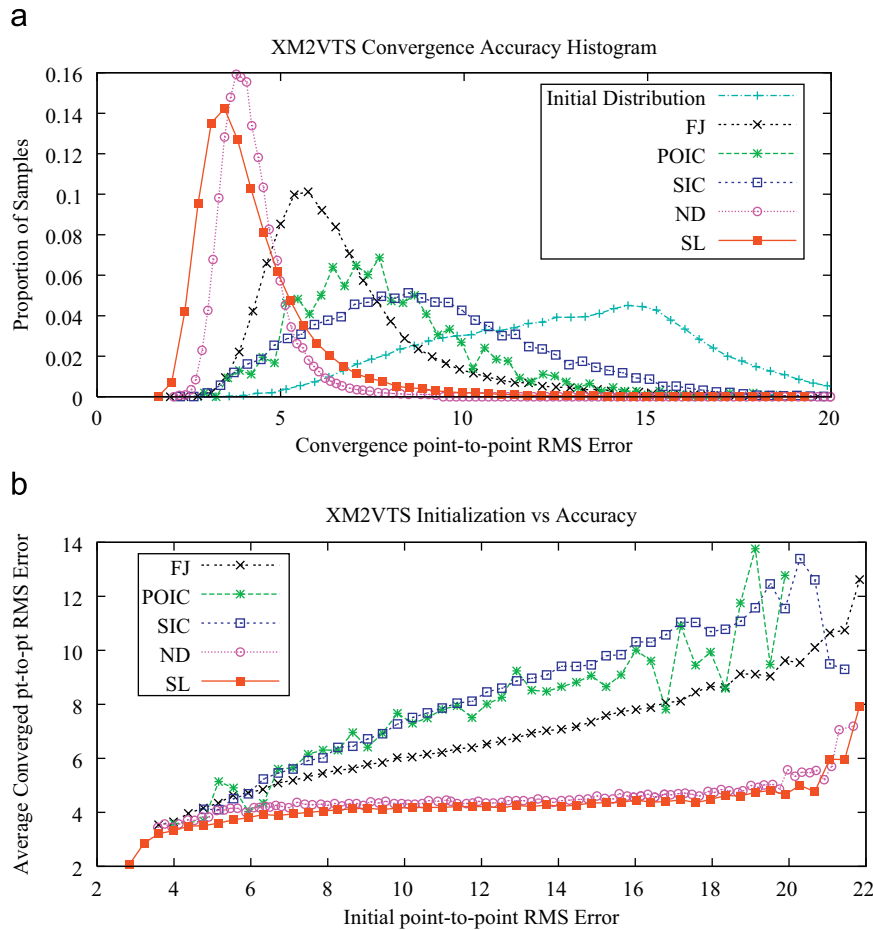


Fig. 3. Convergence performance of the fixed Jacobian (FJ), project-out (POIC), simultaneous inverse compositional (SIC) and the iterative-discriminative methods (SL, ND) on the IMM database. (a) Histograms of accuracy at convergence (percentage in legend is the convergence rate), (b) initial error vs. average convergence accuracy.



**Fig. 4.** Convergence performance of the fixed Jacobian (FJ), project-out (POIC), simultaneous inverse compositional (SIC) and the iterative-discriminative methods (SL, ND) on the XM2VTS database. (a) Histograms of accuracy at convergence (percentage in legend is the convergence rate), (b) initial error vs. average convergence accuracy.

evaluation cost and convergence rate for models in both databases. These values were the smallest for which the optimization remained stable. The step and perturbation decay rates were set to  $\alpha=0.602$  and  $\beta=0.101$ , in accordance with suggestions in [26] (i.e. generic values for SPSA that are not specific to our problem). The initial perturbation size  $\gamma$  was chosen such that the average shape perturbation due to the update model perturbations was around one pixel, a good choice for numerical differentiation on image based functions. The initial step size was set to  $\eta=1.0^{-5}$  with the resulting model update in Eq. (15) scaled according to the maximum magnitude of perturbation.

#### 4.3. Fitting performance

To compare the five methods, the AAM parameters were randomly perturbed from their optimal settings 100 times for each test image in both databases for each of the four trials. The perturbations were sampled as described in Section 4.2, with an additional  $\pm 0.1$ ,  $\pm 20$  and  $\pm 1.5$  standard deviations for the global lighting gain, lighting bias and the intrinsic texture parameters, respectively. FJ, POIC and SIC were fitted using three levels of a Gaussian pyramid to reduce their sensitivity to local minima. SL and ND were fitted to the highest resolution image only, by virtue of their discriminative framework. For SIC, we implemented its efficient approximation proposed in [9], where the Gauss-Newton Jacobian (and, hence, the update models) are precomputed at  $\mathbf{q}_t = \mathbf{0}$ , since the large fitting times for the full approach were impractical for the size the models in our experiments.

**Table 1**

Summary of fitting time and convergence rate.

	IMM		XM2VTS	
	Time (ms)	Rate (%)	Time (ms)	Rate (%)
Fixed Jacobian (FJ) [5]	326	85.7	1437	83.5
Project-out IC (POIC) [6]	193	19.5	454	1.46
Simultaneous IC (SIC) [9]	808	64.3	3189	20.4
Nonlinear discriminative (ND) [11]	403	99.7	823	99.6
Simulation learnt (SL)	125	98.1	284	98.4

The convergence performance of all five methods are presented in Figs. 3 and 4 for the IMM and XM2VTS databases, respectively. In both figures, Plot (a) shows the final accuracy distribution of trials that converged (i.e. a convergence accuracy plot). In Plot (b), the average convergence accuracies of the five methods are plotted against their initial magnitude of perturbation. The convergence rates (i.e. percentage of trails that converged) and average fitting times for each method are presented in Table 1. In all fitting trials, we declare convergence if the final point-to-point RMS error is smaller than at initialization (i.e. the fitting procedure did not diverge). The reported fitting times were obtained from running code, implemented in C++, on a 3 GHz machine with 1 GB of RAM, and does not include the time taken to build the Gaussian pyramids for FJ, POIC and SIC.

On both databases, the overall performance of SL is significantly better than FJ, POIC and SIC, both in convergence rate and accuracy, and comparable to ND. Out of the three generative methods tested, FJ performed the best, achieving a smaller *best error* compared to SL on the IMM database. However, the proportion of samples which achieve this best error is relatively small. Overall, it exhibits a larger proportion of samples at higher convergence errors above 6-pixels RMS compared to SL. On the XM2VTS database, the superiority of SL is even more pronounced. Furthermore, in both databases, the convergence rate of SL is much higher than FJ, achieving a reduction in shape RMS error in almost every trial. Compared to POIC and SIC, again SL boasts a significant performance boost, both in convergence accuracy and rate. This is especially evident in the XM2VTS database where the models exhibit a large number of parameters. Although the inapplicability of POIC for generic face fitting has been previously discussed in [15], results here show that the efficient approximation of SIC also performs poorly in this setting. We suspect the reason for this is to do with the large number of parameters involved in the optimization, as SIC uses an independent appearance model, resulting in a higher likelihood of getting trapped in local minima than FJ, for example. Although a true SIC implementation may improve results, the fitting times required by this method are impractical for the size of the models used for generic face fitting. Even its efficient approximation, which uses a fixed update model, is impractically inefficient. From initial experiments, we found that a full SIC implementation can further increase the processing time by a factor of 10.

Examining Plot (b) of Figs. 3 and 4, the reason for the significant performance improvement achieved by SL compared to the generative methods becomes apparent. The average convergence accuracy of FJ, POIC and SIC deteriorates the further initialization is from the optimum. This is due to their generative fitting regimes, which get trapped in local minima, despite their application on a Gaussian pyramid. In contrast, the deterioration of SL, which was trained discriminatively on simulations of real fitting problems, is not as dramatic, maintaining a good average convergence accuracy up to a capture range of around 20 pixels RMS, which was the maximum translation perturbation used in the training.

The performance of SL and ND in these experiments are comparable. Although the final distribution of samples achieved by ND is more compact it fails to achieve the same levels of accuracy as SL. Despite using a more sophisticated discriminative mapping function, its training regime is suboptimal. The boosting procedure over Haar-like features is essentially a greedy training procedure. As such, the model for each iteration significantly overfits the data, requiring the next iteration to handle the poorly predicted samples.

Despite the significant discrepancy in performance between SL and the generative methods, this performance boost is attained without sacrificing fitting efficiency. This is in contrast to other methods which either sacrifice accuracy for efficiency or vice versa. On a per-iteration basis, SL is slightly faster than POIC, currently the fastest method to date, since it uses the same update form and drives the same number of parameters, but updates the parameters additively rather than in an inverse-compositional fashion. Comparisons of overall fitting speeds depend on the initial perturbation magnitude as well as the error terrain between the initial parameter settings and the optimum. Whereas SL fitting is performed for all the iterations it was trained for, generative fitting procedures generally have an early termination criterion, judged by some measure of parameter convergence. In our experiments, the number of iterations to convergence for POIC is around 10 iterations per pyramid level, whereas SL was trained on 10 iterations at the highest pyramid level only. Furthermore, in practice, there is a computational overhead of building the Gaussian pyramids, which increase the computation time of POIC even further. In any case, the convergence rates of POIC on the two generic face databases tested here is so poor, it negates

the computational advantage of this method for this problem. Finally, SL is roughly three times more efficient than ND.

## 5. Conclusion

We have proposed a new approach to AAM fitting based on simulations of real fitting conditions. This approach boasts significant improvements over the fixed Jacobian, project-out and an efficient approximation of the simultaneous inverse-compositional methods in both convergence accuracy and rate. Furthermore, these improvements are afforded without sacrificing computational efficiency. Also, the method affords excellent generalizability, as evidenced by its high convergence rates.

Another advantage of this formulation is that the fitting procedure can be customized to the detector used for initialization. By building a set of training perturbations which adhere to a prior defined by the detector, better fitting performance may be achieved as the distribution of samples, and hence feature vectors, are more constrained than the uniform random perturbations used in this work.

Finally, it should be noted that the experiments in this work involve a 4-fold cross-validation procedure, separately over each of the databases. Although the results suggest that the proposed approach generalizes well over the types of variations within the training database, little can be said about its generalization between databases. However, such an evaluation is rarely reported in the literature due to the lack of sufficient consistent annotations (i.e. publicly available annotations for different databases are rarely in correspondence). From initial qualitative experiments we found that the performance of all methods evaluated in this work deteriorate significantly when fitting to images from a separate database. This is because the method is required to extrapolate the types of variations exhibited in the training database to those in the testing database. In order to evaluate the generalization of the proposed approach for the case of database invariant fitting, further consistent annotations must be collected. Investigations into this aspect will be the subject of future work.

## References

- [1] G. Edwards, C. Taylor, T. Cootes, Interpreting face images using active appearance models, in: Proceedings of the Third IEEE International Conference on Automatic Face and Gesture Recognition (FG'98), IEEE, Nara, Japan, 1998, pp. 300–305, doi:10.1109/AFGR.1998.670965.
- [2] T. Lehn-Schiöler, L. Hansen, J. Larsen, Mapping from speech to images using continuous state space models, in: Proceedings of the First International Workshop on Machine Learning for Multimodal Interaction (MLMI 2004), Lecture Notes in Computer Science, vol. 3361, Springer, Martigny, Switzerland, 2004, pp. 136–145.
- [3] M. Stegmann, H. Larsson, Fast registration of cardiac perfusion MRI, in: International Society of Magnetic Resonance in Medicine, Toronto, Canada, 2003, p. 702.
- [4] P. Mittrapiyanuruk, G. DeSouza, A. Kak, Accurate 3D tracking of rigid objects with occlusion using active appearance models, in: Proceedings of the IEEE Workshop on Motion and Video Computing (WACV/MOTION 2005), vol. 2, Breckenridge, CO, USA, 2005, pp. 90–95, doi:10.1109/ACVMOT.2005.15.
- [5] T. Cootes, G. Edwards, C. Taylor, H. Burkhardt, B. Neuman, Active appearance models, in: Proceedings of the European Conference on Computer Vision (ECCV'98), Lecture Notes in Computer Science, vols. 2, 1406, Springer, Freiburg, Germany, 1998, pp. 484–498.
- [6] I. Matthews, S. Baker, Active appearance models revisited, International Journal of Computer Vision 60 (2) (2004) 135–164.
- [7] R. Donner, M. Reiter, G. Langs, P. Peloschek, H. Bischof, Fast active appearance model search using canonical correlation analysis, IEEE Transactions on Pattern Analysis and Machine Intelligence 28 (10) (2006) 1690–1694.
- [8] X. Hou, S. Li, H. Zhang, Q. Cheng, Direct appearance models, in: Proceedings of the 2001 IEEE Computer Society Conference on Computer Vision and Pattern Recognition (CVPR 2001), vol. 1, Kauai, HI, USA, 2001, pp. 828–833, doi:10.1109/CVPR.2001.990568.
- [9] S. Baker, R. Gross, I. Matthews, Lucas-Kanade 20 years on: a unifying framework: Part 3, Technical Report, Robotics Institute, Carnegie Mellon University, Pittsburgh, PA, USA, 2003.
- [10] A. Batur, M. Hayes, Adaptive active appearance models, Transactions on Image Processing 14 (11) (2005) 1707–1721.



- [11] J. Saragih, R. Goecke, A nonlinear discriminative approach to AAM fitting, in: Proceedings of the IEEE 11th International Conference on Computer Vision (ICCV 2007), Rio de Janeiro, Brazil, 2007, doi:10.1109/ICCV.2007.4409106.
- [12] S. Zhou, D. Comaniciu, Shape regression machine, in: Proceedings of the 20th International Conference on Information Processing in Medical Imaging (IPMI 2007), Lecture Notes in Computer Science, vol. 4584, Springer, Kerkraade, The Netherlands, 2007, pp. 13–25.
- [13] B. Theobald, I. Matthews, S. Baker, Evaluating error functions for robust active appearance models, in: Proceedings of the 7th International Conference on Automatic Face and Gesture Recognition (FG'06), Southampton, UK, 2006, pp. 149–154, doi:10.1109/FGR.2006.38.
- [14] S. Baker, I. Matthews, Equivalence and efficiency of image alignment algorithms, in: Proceedings of the 2001 IEEE Computer Society Conference on Computer Vision and Pattern Recognition (CVPR 2001), vol. 1, Kauai, HI, USA, 2001, pp. 1090–1097, doi:10.1109/CVPR.2001.990652.
- [15] R. Gross, I. Matthews, S. Baker, Generic vs. person specific active appearance models, *Image and Vision Computing* 23 (12) (2005) 1080–1093.
- [16] X. Liu, Generic face alignment using boosted appearance model, in: Proceedings of the IEEE Conference on Computer Vision and Pattern Recognition (CVPR 2007), Minneapolis, MN, USA, 2007, doi:10.1109/CVPR.2007.383265.
- [17] M. Nguyen, F. De la Torre Frade, Local minima free parameterized appearance models, in: Proceedings of the IEEE Conference on Computer Vision and Pattern Recognition (CVPR 2008), 2008, doi:10.1109/CVPR.2008.4587524.
- [18] O. Williams, A. Blake, R. Cipolla, A sparse probabilistic learning algorithm for real-time tracking, in: Proceedings of the IEEE Ninth International Conference on Computer Vision (ICCV 2003), vol. 1, Beijing, China, 2003, pp. 353–360.
- [19] S. Avidan, Support vector tracking, *IEEE Transactions on Pattern Analysis and Machine Intelligence* 26 (2004) 1064–1072.
- [20] K. Zimmermann, Fast learnable methods for object tracking, Ph.D. Thesis, Czech Technical University, 2008.
- [21] D. Wilson, T. Martinez, The general inefficiency of batch training for gradient descent learning, *Neural Networks* 16 (10) (2003) 1429–1451.
- [22] L. Bottou, Stochastic learning, in: Advanced Lectures on Machine Learning, Lecture Notes in Artificial Intelligence, vol. 3176, Springer, Berlin, 2004, pp. 146–168.
- [23] J. Kivinen, A. Smola, R. Williamson, Online learning with kernels, in: Advances in Neural Information Processing Systems 14 (NIPS 2001), MIT Press, Vancouver, Canada, 2002, pp. 785–793.
- [24] J. Spall, Stochastic optimization: stochastic approximation and simulated annealing, in: J. Webster (Ed.), *Encyclopedia of Electrical and Electronics Engineering*, vol. 20, Wiley, New York, USA, 1998, pp. 529–542.
- [25] J. Spall, Multivariate stochastic approximation using a simultaneous perturbation gradient approximation, *IEEE Transactions on Automatic Control* 37 (3) (1992) 332–341.
- [26] J. Spall, Implementation of the simultaneous perturbation algorithm for stochastic optimization, *IEEE Transactions on Aerospace and Electronic Systems* 34 (3) (1998) 817–823.
- [27] T. Cootes, G. Edwards, C. Taylor, A comparative evaluation of active appearance model algorithms, in: Proceedings of the British Machine Vision Conference (BMVC'98), Southampton, UK, 1998, pp. 680–689.
- [28] J. Saragih, R. Goecke, Iterative error bound minimisation for AAM alignment, in: Proceedings of the 18th International Conference on Pattern Recognition (ICPR 2006), vol. 2, Hong Kong, 2006, pp. 1192–1195, doi:10.1109/ICPR.2006.730.
- [29] D. Liu, J. Nocedal, On the limited memory BFGS method for large scale optimization, *Mathematical Programming* 45 (1–3) (1989) 503–528.
- [30] M. Nordström, M. Larsen, J. Sierakowski, M. Stegmann, The IMM face database—an annotated dataset of 240 face images, Technical Report, Informatics and Mathematical Modelling, Technical University of Denmark, May 2004.
- [31] K. Messer, J. Matas, J. Kittler, J. Lüttin, G. Maitre, XM2VTSDB: the extended M2VTS database, in: Proceedings of the Second International Conference on Audio- and Video-Based Biometric Person Authentication (AVBPA'99), Washington, DC, USA, 1999, pp. 72–77.
- [32] ([http://www.isbe.man.ac.uk/~bim/data/xm2vts/xm2vts\\_markup.html](http://www.isbe.man.ac.uk/~bim/data/xm2vts/xm2vts_markup.html)).

**About the Author**—JASON SARAGIH is a Post-doctoral Research Fellow at the Robotics Institute, Carnegie Mellon University. He received both his undergraduate degree in Systems Engineering and his PhD in Computer Science from the Australian National University, Canberra, Australia, in 2004 and 2008, respectively. His research interests are in pattern recognition, computer vision and human–computer interaction.

**About the Author**—ROLAND GOECKE is a Research Fellow at the Human–Computer Communication Laboratory, Faculty of Information Sciences and Engineering, University of Canberra, and an Adjunct Research Fellow at the Research School of Information Sciences and Engineering, Australian National University, Canberra. He received his Masters degree in Computer Science from the University of Rostock, Germany, in 1998 and his PhD in Computer Science from the Australian National University, Canberra, Australia, in 2004. His research interests are in signal processing, pattern recognition, computer vision, human–computer interaction and affective computing.